

## Electronic Supplementary Information

### **Balancing the Pre-aggregation and Crystallization Kinetics Enables High Efficiency Slot-Die Coated Organic Solar Cells with Reduced Non-radiative Recombination losses**

Baojun Lin <sup>a</sup>, Xiaobo Zhou <sup>a</sup>, Heng Zhao <sup>a</sup>, Jian Yuan <sup>a</sup>, Ke Zhou <sup>a</sup>, Kai Chen <sup>b</sup>, Hongbo Wu <sup>c</sup>, Renjun Guo <sup>d</sup>, Manuel A. Scheel <sup>d</sup>, Andrei Chumakov <sup>e</sup>, Stephan V. Roth <sup>ef</sup>, Yimin Mao <sup>g</sup>, Laili Wang <sup>\*i</sup>, Zheng Tang <sup>\*c</sup>, Peter Müller-Buschbaum <sup>\*dh</sup> and Wei Ma <sup>\*a</sup>

<sup>a</sup>State Key Laboratory for Mechanical Behavior of Materials, Xi'an Jiaotong University, Xi'an 710049, China. E-mail: msewma@xjtu.edu.cn

<sup>b</sup>College of Pharmacy, Xi'an Jiaotong University, Xi'an 710049, China

<sup>c</sup>Center for Advanced Low-dimension Materials, State Key Laboratory for Modification of Chemical Fibers and Polymer Materials, College of Materials Science and Engineering, Donghua University, Shanghai 201620, China. E-mail: ztang@dhu.edu.cn

<sup>d</sup>Technische Universität München, Physik-Department, Lehrstuhl für Funktionelle Materialien, James-Franck-Str. 1, Garching 85748, Germany. E-mail: muellerb@ph.tum.de

<sup>e</sup>Deutsches Elektronen-Synchrotron (DESY), Hamburg 22607, Germany

<sup>f</sup>KTH Royal Institute of Technology, Department of Fibre and Polymer Technology, Teknikringen 56-58, SE-100 44 Stockholm, Sweden

<sup>g</sup>NIST Center for Neutron Research, National Institute of Standards and Technology, 100 Bureau Dr., Gaithersburg, Maryland 20899, United States

<sup>h</sup>Technische Universität München, Heinz Maier-Leibnitz Zentrum (MLZ), Lichtenbergstraße 1, D-85748 Garching, Germany

<sup>i</sup>State Key Laboratory of Electrical Insulation and Power Equipment, Xi'an Jiaotong University, Xi'an 710049, China. E-mail: LLwang@mail.xjtu.edu.cn

## **Experiment section**

### **Materials:**

PM7 is purchased from Solarmer Inc. without further purification and IT4F is synthesized according to the reported literature.

### **Device fabrication:**

The organic solar cells were fabricated with an inverted structure of ITO/ZnO/PM7:IT4F/MoO<sub>3</sub>/Al. The patterned ITO substrates were cleaned by sonication in detergent water, deionized water, acetone and isopropanol for 20 min of each step. After the UVO treatment for 20 min, an electron-transporting layer of ZnO was deposited by spin-coating a ZnO precursor solution at 4500 rpm for 1 min, followed by thermal annealing at 200 °C for 1h. The active layer solution was prepared in chlorobenzene (with 1% DIO by volume) at a total concentration of 22 mg/mL with the D/A ratio of 1:1 by weight, accompanied by string on a hotplate at 50 °C. Then, a ~110 nm active layer was deposited by slot-die coating at the ambient environment. The substrate and die were heated by ceramic heating plates with a closed-loop temperature feedback system. The gap between the bottom of die and substrate was kept as 150 μm. The striping speed was regulated in the range of 6-15 mm/s to obtain similar film thickness. The deposited films were further annealed at 140 °C for 10 min. Finally, a 10 nm MoO<sub>3</sub> and 100 nm Al were sequentially deposited as anode under vacuum ( $<1 \times 10^{-4}$  Pa). The *J-V* characteristics were performed in N<sub>2</sub>-filled glovebox under AM 1.5G (100 mW/cm<sup>2</sup>) by using a Keithley 2400 source meter unit and an AAA solar simulator (SS-F5-3A, Enli Technology CO., Ltd.) calibrated by a standard Si photovoltaic cell with a KG5 filter. The EQE was measured by a solar cell spectral response measurement system (QE-R3018, Enli Technology CO., Ltd.) with the calibrated light intensity by a standard single-crystal Si photovoltaic cell.

### **Characterizations:**

PL, UV-vis, and reflection spectrum measurements. PL spectrum was recorded by FLS980 spectrometer (Edinburgh Instruments, EI). The UV-vis and temperature-dependent UV-vis absorption spectrum was realized by a Shimadzu UV-3600 Plus Spectrophotometer. The *in-situ* UV-vis absorption spectrum was performed by an Ocean Optics QE pro spectrometer using the transmission mode with the time resolution of 0.5 s. The solution concentration was diluted to 2.5 mg/mL due to the limitation of the detector. Film formation time was monitored by the Filmetrics F20-EXR spectrometer using the reflection mode with the time resolution of

0.04 s. The measurements were performed on silicon substrates, using the same solutions as device fabrication.

EL, EQE<sub>el</sub>, sensitive-EQE and TPV measurements. Electroluminescence measurement utilized the direct-current meter (PWS2326, Tectronix) to offer bias voltage to the device, then the luminous signals were collected by fluorescence spectrometer (KYMERA-328I-B2, Andor technology LTD). The EQE-EL measurement system basically included a Keithley 2400 digital source meter, Keithley 6482 picoammeters and a standard Si detector (S1337-1010Br). Transient photovoltage measurements were used to measure the lifetime of charge carriers. The background illumination was provided by a normal LED light source, and pulsed light was provided by arbitrary wave generator (AFG322C, Tektronix), eventually, the transient photovoltage signals for the device was collected by oscilloscope (MDO4104C, Tektronix). For the sensitive-EQE measurement, the light from halogen light source (LSH-75, Newport) became monochromatic light by using a monochromator (CS260-RG-3-MC-A, Newport), and was focused on the device to generate electrical signals. Then the signals were amplified by the front-end current amplifier (SR570, Stanford) and finally collected by the phase-locked amplifier (Newport). The EQE spectrum was obtained by using the corrected Si standard detector (S1337-1010Br). TPV measurement is used to measure the lifetime of carriers. The background illumination was provided by a normal LED light source, and pulsed light was provided by arbitrary wave generator (AFG322C, Tektronix), eventually, the transient photovoltage signals for the device was collected by oscilloscope (MDO4104C, Tektronix).

GIWAXS measurement. Ex-situ GIWAXS measurements were performed at beamline 7.3.3 at the Advanced Light Source. The 10 keV X-ray beam was incident at a grazing angle of 0.11-0.15°, selected to maximize the scattering intensity from the samples. The scattered x-rays were detected using a Dectris Pilatus 2 M photon counting detector. *In-situ* GIWAXS measurements<sup>1</sup> were performed at beamline P03 at the synchrotron PETRA III at Deutsches Elektronen-Synchrotron DESY using a Lambda 750K detector with a pixel size 55×55 μm<sup>2</sup>, X-ray beams size 25×17 μm<sup>2</sup> and wavelength  $\lambda = 1.06 \text{ \AA}$  ( $\Delta\lambda/\lambda = 10^{-4}$ ). Data pretreatment was performed using the software package DPDAK<sup>2</sup>.

RSoXS and SANS measurements. RSoXS transmission measurements were performed at beamline 11.0.1.2 at the Advanced Light Source. Samples for RSoXS measurements were prepared on a PSS modified Si substrate under the same conditions as those used for device

fabrication, and then transferred by floating in water to a 1.5 mm×1.5 mm, 100 nm thick Si<sub>3</sub>N<sub>4</sub> membrane supported by a 5 mm×5 mm, 200 μm thick Si frame (Norcada Inc.). 2D scattering patterns were collected on an in-vacuum CCD camera (Princeton Instrument PI-MTE). The sample detector distance was calibrated from diffraction peaks of a triblock copolymer poly (isoprene-*b*-styrene-*b*-2-vinyl pyridine), which had a known spacing of 391 Å. The beam size at the sample was approximately 100 μm by 200 μm. SANS measurements were performed in American National Institute of Standards and Technology (NIST), with the solution concentration of 11 mg/mL.

TEM and DSC measurements. TEM characterization was performed by a FEI Talos F200c transmission electron microscope at 200 kV. DSC was used to determine phase-transition temperatures on a TA DSC Q20 differential scanning calorimeter with a constant heating rate of 10 °C/min.

Hole and electron mobility measurements. The mobilities were measured by using space charge limited current (SCLC) model with the hole-only device of ITO/PEDOT:PSS/PM7:IT4F/MoO<sub>3</sub>/Al and electron-only device of ITO/ZnO/PM7:IT4F/Ca/Al. Hole mobility and electron mobility were obtained by fitting the current density-voltage curves and calculated by the equation:

$$J = 9\epsilon_0\epsilon_r\mu(V_{appl} - V_{bi} - V_s)^2/8L^3$$

Where  $J$  is current density,  $\epsilon_0$  is the permittivity of free space,  $\epsilon_r$  is the relative permittivity of the material (assumed to 3),  $\mu$  is hole mobility or electron mobility,  $V_{appl}$  is applied voltage,  $V_{bi}$  is the built-in voltage (0 V),  $V_s$  is the voltage drop from the substrate's series resistance ( $V_s = IR$ ) and  $L$  is the thickness of film.

#### Note for energy loss calculation:

The  $V_{oc}$  of any type of solar cells is determined by the ratio between short-circuit current ( $J_{SC}$ ) and dark saturation current ( $J_0$ ), following this expression<sup>3</sup>:

$$V_{OC} = \frac{kT}{q} \ln\left(\frac{J_{SC}}{J_0} + 1\right) \quad (1)$$

where  $k$  is the boltzmann constant,  $T$  is the temperature, and  $q$  is the elementary charge.

The expression for  $J_{SC}$  and  $J_0$  are given by:

$$J_{SC} = q \cdot \int_0^\infty EQE_{PV}(E) \cdot \Phi_{AM1.5}(E) dE \quad (2)$$

$$J_0 = \frac{q}{EQE_{EL}} \cdot \int_0^\infty EQE_{PV}(E) \cdot \Phi_{BB}(E) dE \quad (3)$$

The expression for  $J_0$  is the Rau's reciprocity relation<sup>4</sup>, where  $EQE_{EL}$  is radiative quantum efficiency of the solar cell when charge carriers are injected into the device in dark, and  $\Phi_{BB}$  is the black body spectrum.

When all the recombination is radiative (i.e.  $EQE_{EL}=1$ ),  $J_0$  is minimized, and  $V_{OC}$  is maximized:

$$J_0^{rad} = q \cdot \int_0^\infty EQE_{PV}(E) \cdot \Phi_{BB}(E) dE \quad (4)$$

$$V_{OC}^{rad} = \frac{kT}{q} \ln\left(\frac{J_{SC}}{J_0^{rad}} + 1\right) = \frac{kT}{q} \ln\left(\frac{q \cdot \int_0^\infty EQE_{PV}(E) \cdot \Phi_{AM1.5}(E) dE}{q \cdot \int_0^\infty EQE_{PV}(E) \cdot \Phi_{BB}(E) dE} + 1\right) \quad (5)$$

In the Shockley-Queisser theory<sup>5</sup>, the general quantum efficiency  $EQE_{PV}^{SQ}(E)$  can be defined as follow:

$$EQE_{PV}^{SQ}(E) = 1, E \geq E_{gap}; \quad EQE_{PV}^{SQ}(E) = 0, E < E_{gap} \quad (6)$$

Substituting general quantum efficiency  $EQE_{PV}^{SQ}(E)$  (equation 6) in equation 4, then we can get the saturation current in the SQ limit,  $J_0^{SQ}$ .

$$J_0^{SQ} = q \cdot \int_{E_{gap}}^\infty EQE_{PV}^{SQ}(E) \cdot \Phi_{BB}(E) dE = q \cdot \int_{E_{gap}}^\infty \Phi_{BB}(E) dE \quad (7)$$

In the same way, we can calculate the value of the SQ open-circuit voltage limit,  $V_{OC}^{SQ}$ , according to equation 5,

$$V_{OC}^{SQ} = \frac{kT}{q} \ln\left(\frac{J_{SC}}{J_0^{SQ}} + 1\right) = \frac{kT}{q} \ln\left(\frac{q \cdot \int_0^\infty EQE_{PV}(E) \cdot \Phi_{AM1.5}(E) dE}{q \cdot \int_{E_{gap}}^\infty \Phi_{BB}(E) dE} + 1\right) \quad (8)$$

The difference between  $V_{OC,SQ}$  and  $V_{OC}^{rad}$  is due to that in the SQ theory, the band edge of the absorber is totally abrupt when calculating  $V_{OC}^{rad}$ , the band gap will be smeared out for the existence of charge transfer state absorption.

Therefore, we can deduce the voltage loss of radiative recombination below the gap,  $\Delta V_{OC}^{rad, below gap}$

$$\Delta V_{OC}^{rad, below gap} = V_{OC}^{SQ} - V_{OC}^{rad} \quad (9)$$

The voltage loss due to non-radiative recombination,  $\Delta V_{OC}^{non-rad}$ , can be rewritten as

$$\Delta V_{OC}^{non-rad} = V_{OC}^{rad} - V_{OC} = -\frac{kT}{q} \ln(EQE_{EL}) \quad (10)$$

Based on the previous discussions, we are now able to summarize the energy loss from the  $E_{gap}$  to the  $qV_{OC}$  for any type of solar cells.

$$\begin{aligned} q\Delta V &= \Delta E_1 + \Delta E_2 + \Delta E_3 \\ &= (E_{gap} - qV_{OC}^{SQ}) + q\Delta V_{OC}^{rad, below gap} + q\Delta V_{OC}^{non-rad} \end{aligned} \quad (11)$$

Therefore, we can get these three terms of energy losses based on related experiments and calculations.

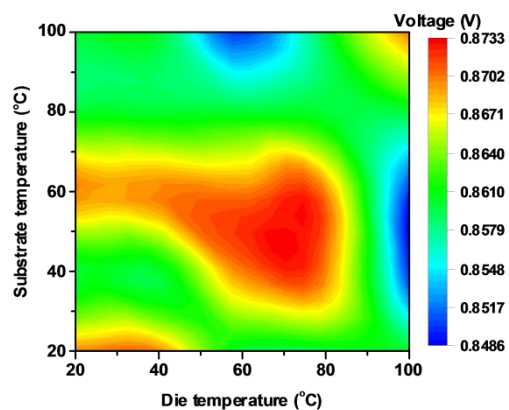


Fig. S1. Contour map of the open circuit voltage of PM7:IT4F devices processed with various die temperatures and substrate temperatures (20, 40, 60, 80 and 100 °C).

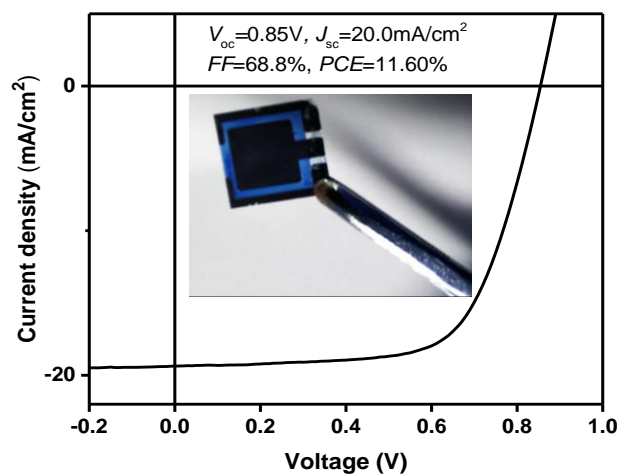


Fig. S2.  $J$ - $V$  curve of the large-area ( $0.95 \text{ cm}^2$ ) device.

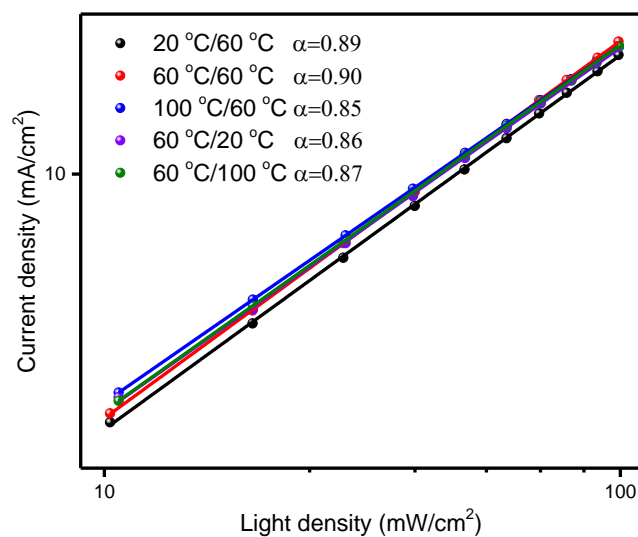


Fig. S3. Dependence of  $J_{sc}$  on light intensity for the PM7:IT4F devices.

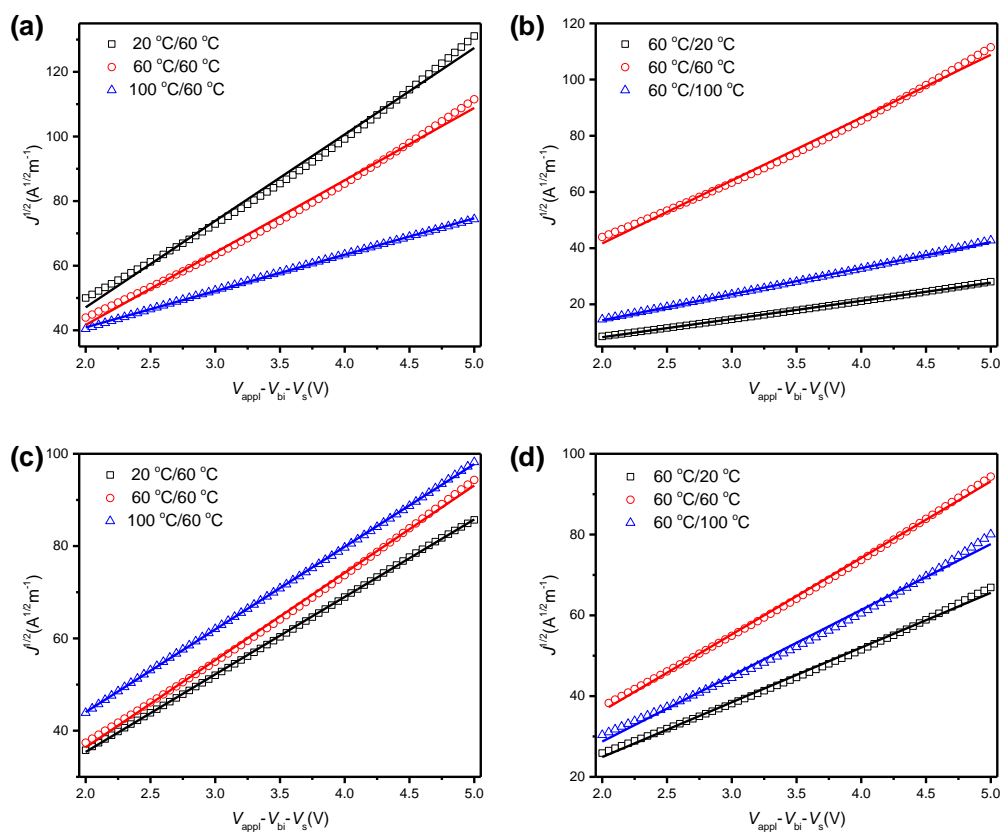


Fig. S4.  $J^{1/2}$ - $V$  characteristics of (a, b) electron-only and (c, d) hole-only devices based on PM7:IT4F devices. The lines present linear fitting results.

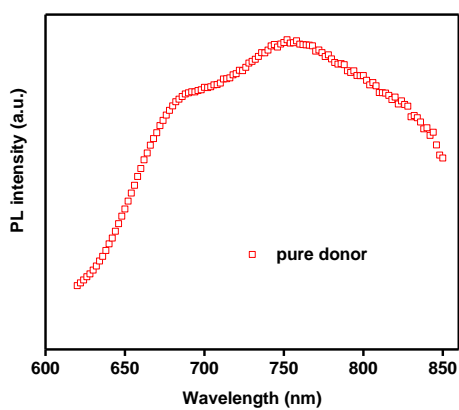


Fig. S5. PL spectrum of the pure PM7 film.

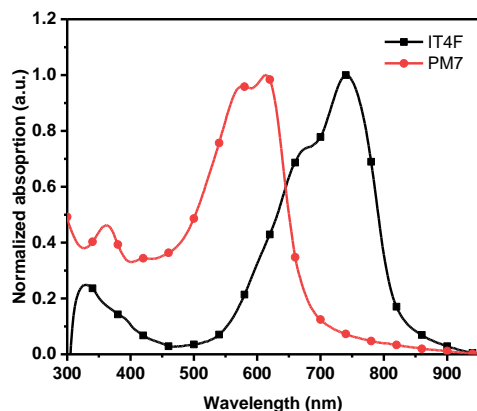


Fig. S6. UV-vis spectrum of the pure PM7 and IT4F film.

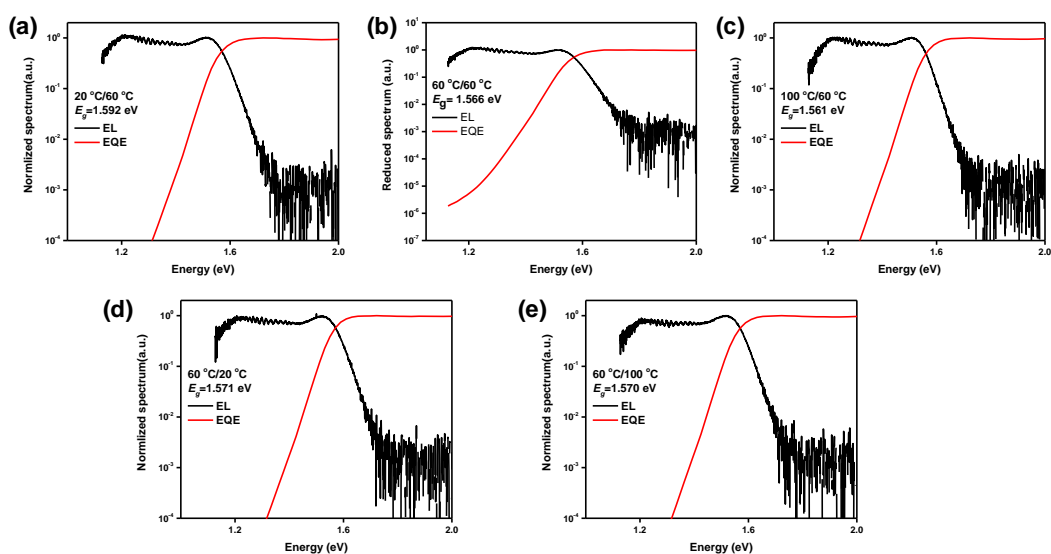


Fig. S7. Normalize EQE and EL spectra of the PM7:IT4F based devices processed at different temperature. (a) 20/60 °C, (b) 60/60 °C, (c) 100/60 °C, (d) 60/20 °C and (e) 60/100 °C.

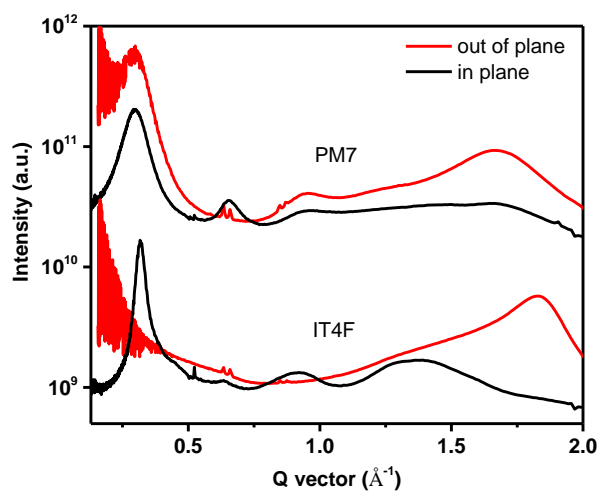


Fig. S8. GIWAXS line profiles of the pure PM7 and IT4F film.

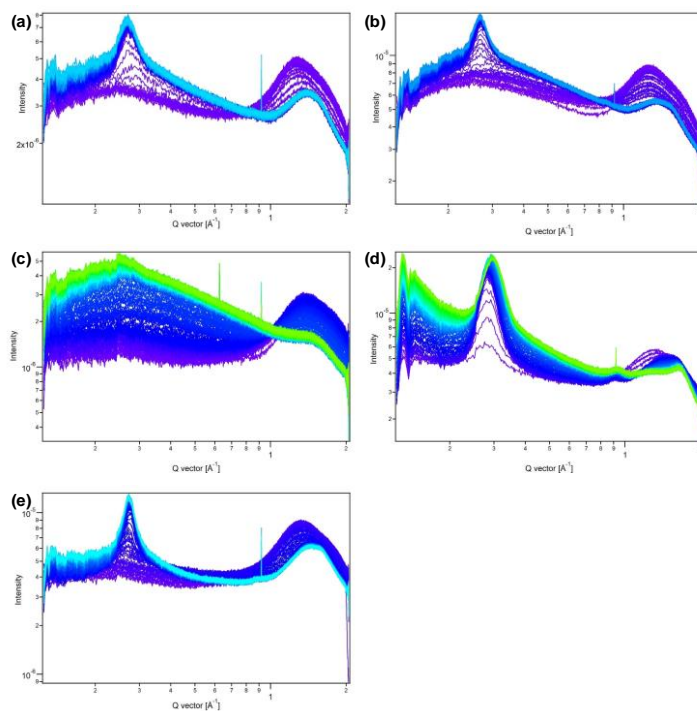


Fig. S9. Time-dependent GIWAXS line profiles of the corresponding films (a) 20/60 °C, (b) 60/60 °C, (c) 60/20 °C, (d) 60/100 °C and (e) 100/60 °C.

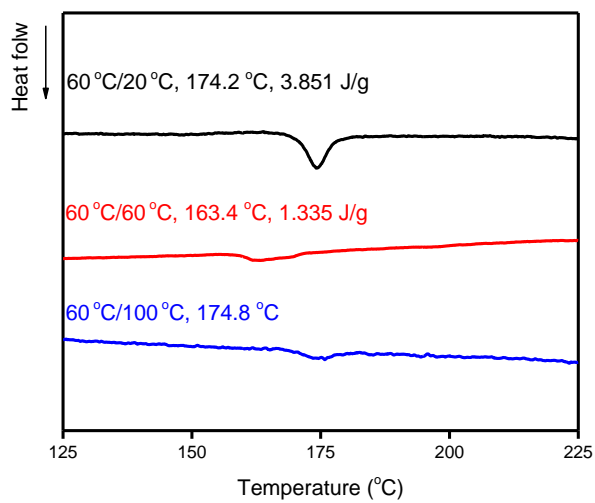


Fig. S10. DSC first heating curves of corresponding samples annealed at 60 °C for two hours.

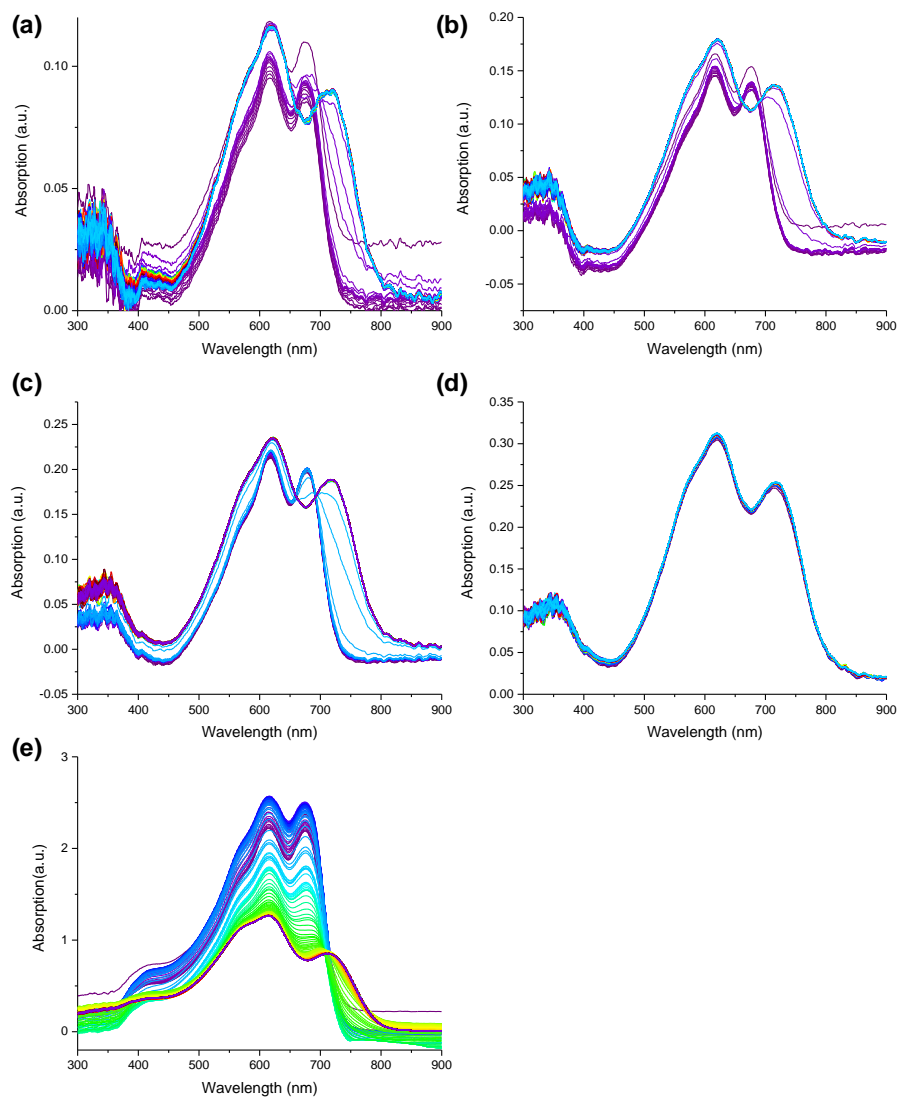


Fig. S11. Time-dependent UV-vis line profiles of the corresponding films (a) 20/60 °C, (b) 60/60 °C, (c) 60/20 °C, (d) 60/100 °C and (e) 100/60 °C.

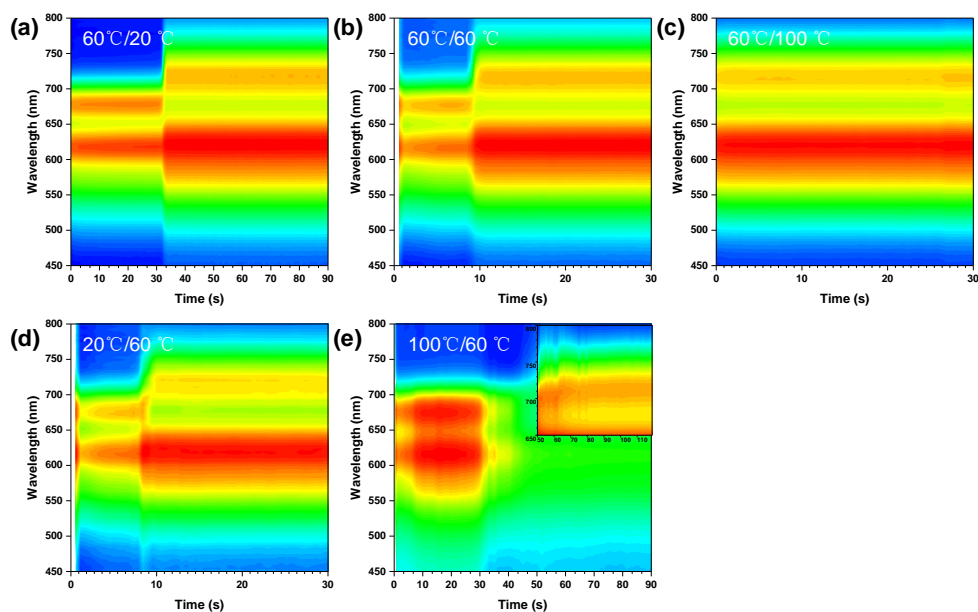


Fig. S12. Contour map of the corresponding films (a) 20/60 °C, (b) 60/60 °C, (c) 100/60 °C, (d) 60/20 °C and (e) 60/100 °C based on the time-dependent UV-vis line profiles

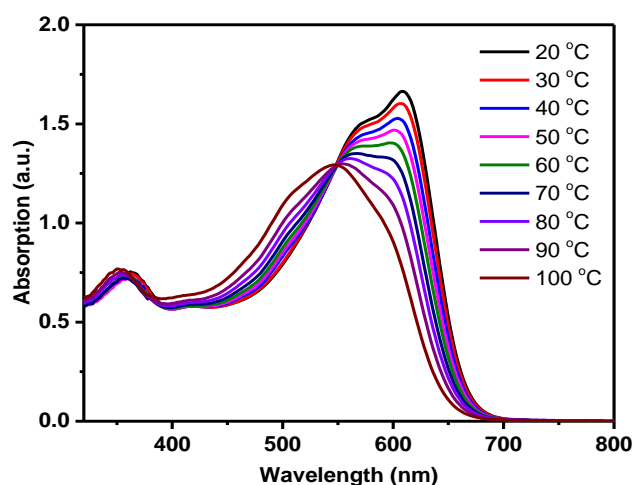


Fig. S13. Temperature-dependent UV-vis absorption spectrum of PM7 solution.

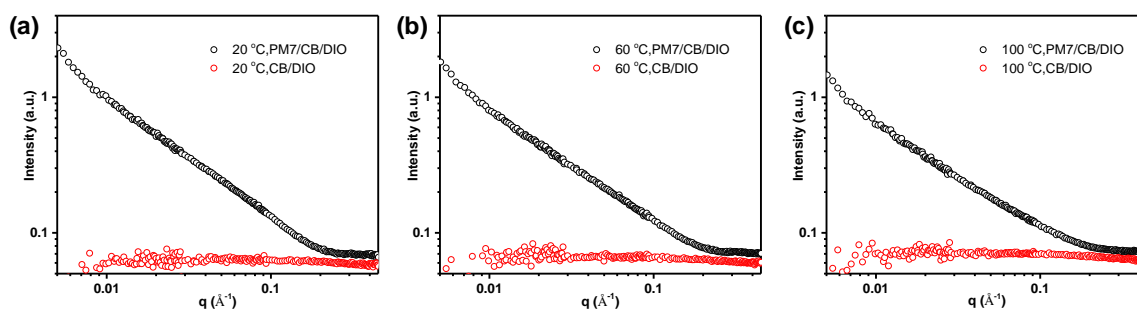


Fig. S14. Raw SANS profiles of PM7 solution at (a) 20 °C, (b) 60 °C and (c) 100 °C.

Table S1. Photovoltaic parameters of the corresponding device (the average values are calculated from 10 devices)

Die Temperature/ Substrate temperature	$V_{oc}$ (V)	$J_{sc}$ (mA/cm <sup>2</sup> )	FF (%)	PCE (%)
20 °C/20 °C	0.87	18.9±0.6	62.0±1.7	10.2±0.1
40 °C/20 °C	0.87	19.4±0.2	62.8±1.7	10.6±0.5
80 °C/20 °C	0.86	22.4±0.8	51.3±1.5	9.7±0.2
100 °C/20 °C	0.86	20.9±0.5	52.7±1.5	9.5±0.2
20 °C/40 °C	0.86	19.1±0.4	68.1±1.6	11.2±0.3
40 °C/40 °C	0.86	19.8±0.6	67.6±1.9	11.5±0.4
60 °C/40 °C	0.87	21.0±0.4	62.9±0.6	11.6±0.2
80 °C/40 °C	0.87	21.2±0.7	55.3±1.0	10.1±0.3
100 °C/40 °C	0.85	21.2±1.1	54.0±2.0	9.7±0.6
40 °C/60 °C	0.87	18.9±0.4	69.4±0.1	11.4±0.2
80 °C/60 °C	0.87	21.6±0.6	60.1±2.0	11.2±0.4
20 °C/80 °C	0.86	20.3±0.9	65.7±1.5	11.4±0.3
40 °C/80 °C	0.86	20.3±0.3	65.3±1.6	11.4±0.2
60 °C/80 °C	0.86	20.8±0.4	66.5±1.2	11.9±0.2
80 °C/80 °C	0.86	21.3±0.2	66.9±1.2	12.2±0.2
100 °C/80 °C	0.86	20.5±0.4	65.5±1.0	11.5±0.4
20 °C/100 °C	0.86	20.7±0.8	65.5±1.5	11.7±0.3
40 °C/100 °C	0.86	20.3±0.7	64.9±1.3	11.3±0.4
80 °C/100 °C	0.86	19.3±0.4	64.4±1.1	11.0±0.4
100 °C/100 °C	0.87	19.2±0.6	66.0±1.9	11.0±0.2

## References

1. A. Buffet, A. Rothkirch, R. Döhrmann, V. Körstgens, M. M. Abul Kashem, J. Perlich, G. Herzog, M. Schwartzkopf, R. Gehrke, P. Müller-Buschbaum, and S. V. Roth, *J. Synchr. Radiation*, 2012, **19**, 647.
2. G. Benecke, W. Wagermaier, C. Li, M. Schwartzkopf, G. Flucke, R. Hoerth, I. Zizak, M. Burghammer, E. Metwalli, P. Müller-Buschbaum, M. Trebbin, S. Förster, O. Paris, S. V. Roth, and P. Fratzl, *J. Appl. Cryst.*, 2014, **47**, 1797.

3. K. Vandewal, K. Tvingstedt, A. Gadisa, O. Ingans and J. V. Manca, *Nat Mater*, 2009, 8, 904-909.
4. U. Rau, *Physical Review B*, 2007, 76, 85303.
5. W. Shockley and H. J. Queisser, *Journal of Applied Physics*, 1961, 32.